J. LANG AND W. MERZ[1]

Two–Dimensional Adaptive Simulation of Dopant Diffusion in Silicon

[1] Technische Universität München, Arcisstr. 21, D–80333 München, Germany

TWO–DIMENSIONAL ADAPTIVE SIMULATION OF DOPANT DIFFUSION IN SILICON

JENS LANG[†] AND WILHELM MERZ[‡]

Abstract. One important step in the fabrication of silicon–based integrated circuits is the creation of semiconducting areas by diffusion of dopant impurities into silicon. Complex models have been developed to investigate the redistribution of dopants and point defects. In general, numerical analysis of the resulting PDEs is the central tool to assess the modelling process. We present an adaptive approach which is able to judge the quality of the numerical approximation and which provides an automatic mesh improvement. Using linearly implicit methods in time and multilevel finite elements in space, we are able to integrate efficiently the arising reaction–drift–diffusion equations with high accuracy. Two different diffusion processes of practical interest are simulated.

Key words. Semiconductor devices, nonlinear reaction–drift–diffusion equations, mesh control, multilevel finite elements, Rosenbrock methods.

AMS subject classifications. 35J60, 35K45, 35K57, 65L06, 65M60, 65N50.

1. Introduction. Semiconductor device simulations which utilize sound physical models are nowadays an attractive tool to create new generations of devices. The permanent advance in computational capabilities allows the incorporation of more and more detailed physics into higher dimensional models in oder to remain relevant for research efforts. Due to the great complexity of the established models, the numerical analysis of PDEs is the central tool to assess the modelling process for large scale problems. From our perspective, the most important requirement that modern simulation programs must meet today is that they are able to judge the quality of their numerical approximations and to determine an adaptive strategy to improve the accuracy where needed. In such a way numerical and modelling errors can be clearly distinguished with the effect that the reliability of the modelling process can be assessed. Moreover, successful adaptive methods lead to substantial savings in computational work. The motivation of our work in this field has been our conviction that although engineering programs like SUPREM-IV (see [4] and references therein), DIOS [8], and PROMIS [21], are very useful tools they are only as reliable as the accuracy of their numerical solutions can be assessed safely.

After presenting a representative survey of simulation software CAREY ET AL. [4] pointed out that there is nowadays an increasing emphasis on all aspects of adaptively generating a grid that evolves with the solution. Another challenge mentioned there is to develop efficient higher–order one–step integration methods which can handle very stiff reaction–diffusion problems and which allow us to accommodate a grid and a moving boundary in each time step without any specific difficulties. In this work we present a combination of both error–controlled grid refinement and powerful one–step methods of linearly implicit type.

An elementary process step in the fabrication of silicon–based integrated circuits is the diffusion mechanism of dopant impurities into silicon. The study of diffusion processes is of great technological importance since their quality strongly influences

---

[†]Konrad–Zuse Zentrum fuer Informationstechnik, Takustr. 7, D–14195 Berlin–Dahlem, Germany (`lang@zib.de`).

[‡]Technische Universitaet Muenchen, Arcisstr. 21, D–80333 Muenchen, Germany (`merz@appl-math.tu-muenchen.de`).

the quality of electronical materials. Impurity atoms of higher or lower chemical valence, such as arsenic, phosphorus, and boron, are introduced under high temperatures ($900°C$–$1100°C$) into a silicon crystal to change its electrical properties. This is the central process of modern silicon technology. Various pair–diffusion models have been developed to allow accurate modelling of device processing. A good survey is given by FAHEY, GRIFFIN and PLUMMER [9], where also a substantial bibliography on the subject can be found. It should be pointed out that there is also an increasing activity in mathematics to analyse the properties of such models, including existence, uniqueness, and regularity of their solutions (e.g. GLIZTKY and HÜNLICH [11], MERZ ET AL. [18, 19]).

In this work, we select two different problems arising in current modelling of dopant diffusion in semiconductor device simulations and demonstrate the new perspective that is opened by a dynamic error control. The simulation of the selected dopant diffusion models requires the numerical solution of systems of time–dependent partial differential equations involving algebraic equations as well. Due to the highly nonuniformity of information distributed in time and space a self–adaptive algorithm is often the only way to get an accurate solution with an acceptable amount of computational time and memory requirement. We have used the finite element program package KARDOS which was developed at the Konrad–Zuse–Zentrum in Berlin to solve general nonlinear evolution problems in an adaptive way (ROITZSCH, ERDMANN, and LANG [24]). In contrast to the widely used method of lines approach the code is based on the adaptive Rothe method employing the discretization sequence first in time and then in space (BORNEMANN [2], LANG [16, 17]). Multilevel techniques as proposed by DEUFLHARD, LEINEN, and YSERENTANT [6] are used to improve the spatial discretization in each time step, utilizing robust a posteriori error estimates of the current solution. For the time discretization, linearly implicit methods of Rosenbrock type with an error–controlled step size selection is applied. These features free us from designing fixed spatial meshes where a priori knowledge about the regions of main activities is required, and from tuning various solution parameters. It is our strong feeling that a fully adaptive approach is always a valuable tool to perform computations in a safe manner and allows the user to concentrate on the evaluation, comparison, and verification of the different physical models.

This paper is organized as follows. We first introduce in Section 2 the reaction–drift–diffusion model in the two–dimensional case. In Section 3, we describe our adaptive time and space discretizations. In Section 4, two different dopant diffusion models are introduced and numerical simulations are presented.

2. The Reaction–Drift–Diffusion Model. We consider m species X_i, $i = 1, \ldots, m$, and distinguish between mobile and immobile ones, introducing two index sets I and I', where $I \cup I' = \{1, \ldots, m\}$ and $I \cap I' = \emptyset$. Each X_i is considered as a union of charged species $X_i^{(j)}$, with $j \in S_i := \{-N_i, \ldots, M_i\}, N_i, M_i \in \mathbb{N}$. Specially, immobile species possess only one constant charge state. Denoting by C_i the total concentration of X_i, $i = 1, \ldots, m$, we set for the mobile and immobile species

$$(2.1) \qquad C_i := \sum_{j \in S_i} C_i^{(j)}, \quad i \in I \cup I',$$

where $C_i^{(j)}$ denotes the concentration of $X_i^{(j)}$, and we write $\boldsymbol{C} = (C_1, \ldots, C_m)^T$ for the whole concentration vector. Clearly, the consideration of the total concentration only

reduces drastically the number of equations (we get m instead of $\sum_{i=1}^{m}(N_i + M_i + 1)$ equations) as well as the physical constants necessary to describe the models appearing in modern semiconductor device simulations. In the case of phosphorus diffusion in silicon, the precise derivation and physical meaning of all the averaged quantities can be found in GHADERI & HOBLER [10] and HÖFLER & STRECKER [14]. There it is also shown that each individual concentration $C_i^{(j)}$ in (2.1) can directly be computed from the total concentration C_i, $i \in I \cup I'$.

We assume that the charge density of the electrons n and the holes p obey the Boltzmann statistics

$$(2.2) \qquad n = n_i \exp\left(\frac{\psi}{U_T}\right), \qquad p = n_i \exp\left(-\frac{\psi}{U_T}\right),$$

where n_i stands for the intrinsic carrier concentration, ψ denotes the chemical potential of the electrons, and U_T is the thermal voltage defined by $U_T = k_B T_a/e$ with the Boltzmann constant k_B, the absolute temperature T_a, and the elementary charge e.

Defining the total reference concentrations

$$(2.3) \qquad P_i(\psi) := \sum_{j \in S_i} K_i^j \exp(-j\psi/U_T), \quad i \in I \cup I',$$

where K_i^j are positive constants, we introduce the electro–chemical activity u_i of each species X_i by

$$(2.4) \qquad u_i := C_i/P_i(\psi), \quad i \in I \cup I'.$$

We set $\Omega_T := \Omega \times (0,T)$, where $\Omega \subset \mathbb{R}^2$, $0 < T < \infty$, and define $\Sigma_T := \partial\Omega \times (0,T)$ which is composed of two disjoint parts for each mobile species, say Σ_{T,N_i} and Σ_{T,D_i}, $i \in I$. The reaction–drift–diffusion model supplemented with physically motivated boundary and initial conditions splits into reaction–diffusion equations for the mobile species X_i, $i \in I$,

$$(2.5) \quad \begin{cases} \dfrac{\partial C_i}{\partial t} + \operatorname{div} J_i(\boldsymbol{C}, \psi) + R_i(\boldsymbol{C}, \psi) &=& 0 & \text{in } \Omega_T, \\[2mm] J_i(\boldsymbol{C}, \psi) \cdot \boldsymbol{n} &=& h_i(\psi)(C_i - P_i(\psi)) & \text{on } \Sigma_{T,N_i}, \\[2mm] C_i &=& P_i(\psi) & \text{on } \Sigma_{T,D_i}, \\[2mm] C_i(t=0) &=& C_i^0 & \text{in } \Omega, \end{cases}$$

reaction equations for the immobile species X_i, $i \in I'$,

$$(2.6) \quad \begin{cases} \dfrac{\partial C_i}{\partial t} + R_i(\boldsymbol{C}, \psi) &=& 0 & \text{in } \Omega_T, \\[2mm] C_i(t=0) &=& C_i^0 & \text{in } \Omega, \end{cases}$$

and a Poisson equation for the chemical potential ψ of the electrons

4

$$\begin{cases} -\dfrac{\varepsilon}{e}\,\triangle\,\psi + 2n_i \sinh\left(\dfrac{\psi}{U_T}\right) - \displaystyle\sum_{i=1}^{m} Q_i(\psi)C_i &=& 0 \quad \text{in } \Omega_T\,, \\[2ex] \nabla\psi\cdot\boldsymbol{n} &=& 0 \quad \text{on } \Sigma_T\,, \end{cases}$$
(2.7)

where ε is the dielectric constant. Here, J_i denote the drift–diffusion terms, R_i are the generation–recombination rates, Q_i are the total charges, and h_i are the transition coefficients.

The standard model for the drift–diffusion term corresponds to

$$J_i = -D_i(\psi)\left(\nabla C_i + Q_i(\psi)C_i\nabla\left(\dfrac{\psi}{U_T}\right)\right)\,,\quad i\in I\,,$$
(2.8)

with the total diffusivity

$$D_i(\psi) = \sum_{j\in S_i} D_i^j K_i^j \exp\left(-j\psi/U_T\right) / P_i(\psi)\,,$$
(2.9)

where D_i^j are positive constants. The total charge $Q_i(\psi)$ is determined by

$$Q_i(\psi) = \sum_{j\in S_i} jK_i^j \exp\left(-j\psi/U_T\right) / P_i(\psi)$$
(2.10)

and the transition coefficients read

$$h_i(\psi) = \sum_{j\in S_i} h_i^j K_i^j \exp\left(-j\psi/U_T\right) / P_i(\psi)\,,$$
(2.11)

where h_i^j are non–negative constants. The source terms $R_i(\boldsymbol{C},\psi)$ result from the reactions occurring during the redistribution of the immobile species. From the mass action law we get

$$\alpha_1 X_1 + \ldots + \alpha_m X_m \rightleftharpoons \beta_1 X_1 + \ldots + \beta_m X_m\,,$$
(2.12)

where the stoichiometric coefficients $\boldsymbol{\alpha} := (\alpha_1,\ldots,\alpha_m)$, $\boldsymbol{\beta} := (\beta_1,\ldots,\beta_m) \in Z_+^m$ represent a special reaction taken from a certain set of permissible reactions $\mathcal{R} \subset Z_+^m \times Z_+^m$. Using the abbreviation $\boldsymbol{u}^{\boldsymbol{\alpha}} := \Pi_{i=1}^m u_i^{\alpha_i}$, the reaction rates R_i have the concrete form

$$R_i(\boldsymbol{C},\psi) = \sum_{(\boldsymbol{\alpha},\boldsymbol{\beta})\in\mathcal{R}} (\alpha_i - \beta_i)\,K_{\boldsymbol{\alpha}\boldsymbol{\beta}}(\psi)\left(\boldsymbol{u}^{\boldsymbol{\alpha}} - \boldsymbol{u}^{\boldsymbol{\beta}}\right)$$
(2.13)

with the total reaction rate coefficients $K_{\boldsymbol{\alpha}\boldsymbol{\beta}}(\psi)$.

The well–posedness of system (2.5)–(2.7) under general assumptions has been investigated by MERZ ET AL. [18, 19].

3. Time and Space Discretization. The system of equations (2.5)–(2.7) can be written in the form of a quasilinear initial–value problem

$$(3.1) \qquad \begin{cases} H\,\dfrac{\partial \boldsymbol{v}}{\partial t} + \operatorname{div} \boldsymbol{J}(\boldsymbol{v}) + \boldsymbol{R}(\boldsymbol{v}) &=\; 0 \quad \text{in } \Omega_T\,, \\[2mm] \boldsymbol{v}(t=0) &=\; 0 \quad \text{in } \Omega\,, \end{cases}$$

where $\boldsymbol{v} = (C_1, \ldots, C_m, \psi)^T$ is the $(m+1)$–dimensional solution vector. The $(m+1) \times (m+1)$–matrix H is diagonal and has one zero entry, i.e., $H = \operatorname{diag}(1, \ldots, 1, 0)$, showing that the system is of differential–algebraic structure. The components of the flux vector $\boldsymbol{J}(\boldsymbol{v}) = (J_1(\boldsymbol{v}), \ldots, J_{m+1}(\boldsymbol{v}))$ that correspond to the immobile species X_i, $i \in I'$, vanish whereas the remaining diffusion operators are supplemented with the corresponding boundary conditions given in (2.5) and (2.7). The reaction vector $\boldsymbol{R}(\boldsymbol{v})$ can be derived analogously. An initial value for ψ has to be calculated from the elliptic equation in (2.7) using the starting values for the concentration vector $\boldsymbol{C}$.

The principle difficulties in solving the system (3.1) numerically are the strong nonlinearities, the differential–algebraic structure, and the presence of differential operators making the problem infinitely stiff. In such a situation, an implicit or semi–implicit discretization method should be applied to integrate in time. We use linearly implicit methods of Rosenbrock type which are constructed by working the exact Jacobian directly into the formula – an idea which was first proposed by ROSENBROCK [25]. Applied to (3.1) a so–called s–stage Rosenbrock method has the recursive form

$$(3.2) \quad \begin{cases} \boldsymbol{v}_n \;=\; \boldsymbol{v}_{n-1} + \displaystyle\sum_{i=1}^{s} b_i \boldsymbol{V}_i^n\,, \\[4mm] \left(\dfrac{H}{\gamma \tau_n} + A(\boldsymbol{v}_{n-1})\right) \boldsymbol{V}_i^n \;=\; \displaystyle\sum_{j=1}^{i-1} \dfrac{c_{ij}}{\tau_n} H \boldsymbol{V}_j^n - \operatorname{div} \boldsymbol{J}\left(\boldsymbol{v}_{n-1} + \sum_{j=1}^{i-1} \alpha_{ij} \boldsymbol{V}_j^n\right) \\[4mm] \hspace{3cm} - \boldsymbol{R}\left(\boldsymbol{v}_{n-1} + \displaystyle\sum_{j=1}^{i-1} \alpha_{ij} \boldsymbol{V}_j^n\right)\,, \quad i = 1, \ldots, s\,, \end{cases}$$

where $\boldsymbol{v}_n$ denotes an approximation of $\boldsymbol{v}(t_n)$ at $t_n = \sum_{i=1,\ldots,n} \tau_i$ and A is the Jacobian matrix $\partial(\operatorname{div}\boldsymbol{J}(\boldsymbol{v}) + \boldsymbol{R}(\boldsymbol{v}))/\partial \boldsymbol{v}$. The coefficients γ, α_{ij}, c_{ij}, and b_i are suitable chosen to obtain good stability properties for stiff equations and a desired order of consistency. In this work we have used the Rosenbrock solver ROWDA3 proposed by ROCHE [23]. The corresponding coefficients are presented in Tab. 3.1.

The fundamental idea of linearly implicit methods is that for the calculation of the intermediate values $\boldsymbol{V}_i^n$, $i = 1, \ldots, s$, only a sequence of linear systems with one and the same operator have to be solved. An iterative Newton method as known from (fully) implicit time discretizations is no longer required. More details can be found in the books of STREHMEL & WEINER [26], HAIRER & WANNER [13], and DEUFLHARD & BORNEMANN [5].

The specific structure of the Rosenbrock method (3.2) allows us to construct a second solution of inferior order

$$(3.3) \qquad \boldsymbol{v}_n^* = \boldsymbol{v}_{n-1} + \sum_{i=1}^{s} b_i^* \boldsymbol{V}_i^n\,,$$

replacing the coefficients b_i in (3.2) by a different set of coefficients b_i^*. The difference between the two solutions is then used to estimate the local temporal error by

$$(3.4) \qquad\qquad \epsilon_n := \| \boldsymbol{v}_n - \boldsymbol{v}_n^* \|_\Omega \, .$$

In practical applications it is often decisive to choose the norm carefully in order to reflect accurately the scale of the problem. We employ here the weighted root mean square norm

$$(3.5) \qquad \| \boldsymbol{v}_n - \boldsymbol{v}_n^* \|_\Omega := \left(\frac{1}{m+1} \sum_{i=1}^{m+1} \frac{\| v_{n,i} - v_{n,i}^* \|_{L_2(\Omega)}^2}{w_i^2} \right)^{1/2}$$

with weights

$$(3.6) \qquad\qquad w_i = \mathrm{ATOL}_i \, + \, \| U_{n,i} \|_{L_2(\Omega)} \cdot \mathrm{RTOL}_i \, .$$

Here, $\boldsymbol{U}_n = (U_{n,1}, \ldots, U_{n,m+1})$ should be a good approximation to the actual solution at $t = t_n$. The tolerances ATOL_i and RTOL_i have to be selected carefully to furnish meaningful input for the error control.

$\gamma \quad = \quad 4.358665215084590e-01$	
$\alpha_{21} = \quad 1.605996252195329e+00$	$c_{21} = 8.874044410657833e-01$
$\alpha_{31} = \quad 1.605996252195329e+00$	$c_{31} = 2.398747971635036e+01$
$\alpha_{32} = \quad 0.000000000000000e+00$	$c_{32} = 5.263722371562129e+00$
$b_1 \quad = \quad 2.236727045296590e+00$	$b_1^* \quad = 2.059356167645940e+00$
$b_2 \quad = \quad 2.250067730969644e+00$	$b_2^* \quad = 1.694014319346528e-01$
$b_3 \quad = -2.092514044390320e-01$	$b_3^* \quad = 0.000000000000000e+00$

FIG. 3.1. *Set of coefficients for the 3-stage* ROWDA3 *method.*

Given a tolerance TOL_t for the time discretization, a standard strategy is to choose the step size of the time step according to

$$(3.7) \qquad\qquad \tau_{n+1} = \frac{\tau_n}{\tau_{n-1}} \left(\frac{\mathrm{TOL}_t \cdot \epsilon_{n-1}}{\epsilon_n \cdot \epsilon_n} \right)^{1/p} \tau_n \, ,$$

where $p-1$ is the order of the second solution $\boldsymbol{v}_n^*$. The proposed step τ_{n+1} is then executed. If the new error ϵ_{n+1} computed from (3.4) is less than TOL_t the solution $\boldsymbol{v}_{n+1}$ is accepted. Otherwise, the solution is rejected and the time step is repeated with a reduced value of τ_{n+1}. Formula (3.7) is related to a discrete PI–controller first established by GUSTAFSSON ET AL. [12].

The linear problems (3.2) have to be solved for the intermediate values $\boldsymbol{V}_i^n$, $i = 1, \ldots, s$. To get the right boundary conditions for those components that correspond to the mobile species and the chemical potential, the Rosenbrock scheme

(3.2) must be also applied to the non–linear algebraic equations describing the solution on the boundary. The arising elliptic boundary value problems are solved by a multilevel finite element method. The main idea of the multilevel technique consists of replacing the solution space by a sequence of discrete spaces with successively increasing dimensions to improve the approximation property. It has proven to be a useful tool for drastically reducing the size of the arising linear systems and to achieve high and controlled accuracy of the spatial discretization (see e.g. DEUFLHARD, LEINEN, and YSERENTANT [6], BORNEMANN, ERDMANN, and KORNHUBER [3]).

The starting point of the finite element method is the weak formulation of (3.2). Let Ω_h be a permissible triangulation of $\Omega \subset \mathbb{R}^2$ into triangles and let S_h^1 consists of all continuous vector functions the components of which are polynomials of first order on each triangle. The finite element approximations $\boldsymbol{V}_{i,h}^n \in S_h^1$, $i = 1, \ldots, s$, have then to satisfy the equations

$$(3.8) \qquad \left(L_n \boldsymbol{V}_{i,h}^n, \boldsymbol{\phi} \right) = \left(\boldsymbol{r}_i^n, \boldsymbol{\phi} \right) \quad \text{for all } \boldsymbol{\phi} \in S_h^1 \,,$$

where L_n is the weak representation of the differential operator at the left–hand side in (3.2) and $\boldsymbol{r}_i^n$ stands for the entire right–hand side of the i–th equation in (3.2). Since the operator L_n is independent of i its calculation is required only once within each time step.

After computing the approximate intermediate values, a posteriori error estimators can be utilized to give specific assessment of the error distribution. In the spirit of BABUŠKA & RHEINBOLDT [1], the spatial errors $\boldsymbol{e}_i^n = \boldsymbol{V}_i^n - \boldsymbol{V}_{i,h}^n$ are estimated by solving local Dirichlet problems on small subdomains. Let ω be the union of two triangles having one common edge and let Q_ω consists of all continuous vector functions the components of which are polynomials of second order on each triangle belonging to ω. The local errors $\boldsymbol{e}_i^n$ are then approximated by $\boldsymbol{e}_{i,h}^n \in Q_\omega$ satisfying

$$(3.9) \quad \begin{cases} \left(L_n \boldsymbol{e}_{i,h}^n, \boldsymbol{\phi} \right) & = & \left(\boldsymbol{r}_i^n (\boldsymbol{e}_{1,h}^n + \boldsymbol{V}_{1,h}^n, \ldots, \boldsymbol{e}_{i-1,h}^n + \boldsymbol{V}_{i-1,h}^n) - L_n \boldsymbol{V}_{i,h}^n, \boldsymbol{\phi} \right) \,, \\ \boldsymbol{e}_{i,h}^n & = & 0 \quad \text{on } \partial\omega \,, \quad i = 1, \ldots, s \,, \end{cases}$$

for all $\boldsymbol{\phi} \in Q_\omega$.

Once the approximate local spatial errors have been computed, we can estimate the local error of the discrete Rosenbrock solution $\boldsymbol{v}_{n,h} = \boldsymbol{v}_{n-1,h} + \sum_{i=1,\ldots,s} b_i \boldsymbol{V}_{i,h}^n$ by

$$(3.10) \qquad \eta := \left\| P\boldsymbol{v}_{n-1,h} + \sum_{i=1}^s b_i \boldsymbol{e}_{i,h}^n \right\|_\omega \,.$$

Here, $P\boldsymbol{v}_{n-1,h}$ stands for the projection error resulting from representing the old solution $\boldsymbol{v}_{n-1,h}$ on the new mesh designed for $\boldsymbol{v}_{n,h}$. The error estimator η is an asymptotically upper bound for the norm of the local error. At first glance, it should be attractive to use an increased size of the domain ω to improve the quality of the error estimator. However, the extensive comparison done by MITCHELL [20] shows that the increased effort caused by solving local problems with more degrees of freedom often does not pay off.

The estimation procedure is applied all over the computational domain, in our case to all ω_k defined by the edges of Ω_h. In order to produce a nearly optimal finite

element mesh, subdomains ω_k having an error η_k larger than the mean square value of all errors are refined. Triangles marked for refinement are divided into four congruent triangles (*red* refinement). After that triangles with two or three refined edges are compulsorily refined *red*; triangles with only one refined edge are subdivided into two triangles (*green* closure). *Green* elements are removed before the next refinement to avoid bad geometric properties of the triangulation. This refinement strategy is standard and used e.g. in the KASKADE code [7].

The refinement technique described above equilibrates the local error over the whole mesh in several iterations and improves the finite element solution until a fixed spatial tolerance

$$(3.11) \qquad \left(\sum_k \eta_k^2 \right)^{1/2} \leq \mathrm{TOL}_x$$

is achieved. Coarsening takes place only after an accepted time step before starting the multilevel process. We identify regions of small errors by their η–values. We coarse a region ω if η does not exceed a quarter of the mean square value of all η_k computed for the finest mesh.

In practical computations the temporal and spatial discretization error have to be balanced to keep the entire error below a prescribed tolerance TOL. We set $\mathrm{TOL}_t = \mathrm{TOL}/2$ and $\mathrm{TOL}_x = \mathrm{TOL}/3$, which worked quite well for the problems we have solved. The linear systems are solved by the BICGSTAB–algorithm [27] preconditioned with an ILU–method.

4. Numerical Simulations. In order to test our dynamic mesh design algorithm, a series of simulations for two different physical models have been performed. We first consider the interaction of two unequally charged dopants, arsenic and boron, and the influence of the chemical potential ψ. The second model describes phosphorus diffusion. It is based on a so–called pair–diffusion mechanism. Point defects such as interstitials and vacancies influence the diffusion process under high temperatures $(900°C–1100°C)$. We concentrate on a comparison of our results with those known from literature (e.g. [10], [14], and [15]). It turns out that practically relevant problems of the present type can safely and efficiently be solved by the proposed adaptive approach.

We have solved the dopant diffusion processes on the rectangle $\Omega = \{ \boldsymbol{x} = (x_1, x_2) \in \mathbb{R}^2, 0 < x_1 < 10^{-3}, 0 < x_2 < 10^{-4} \}$ for $t > 0$, where the unit of measurement is given in cm. The wafer surface is located at $x_1 = 0$ and the bottom of the wafer is at $x_2 = 10^{-3}$. The relatively large expansion of the computational domain guarantees that the solution is not affected by the boundary conditions at the bottom.

The implanted dopant concentrations are set initially to Gaussian profiles of the form

$$(4.1) \qquad C_i(\boldsymbol{x}, 0) = \tilde{C}_i \exp \left(-\frac{f(\boldsymbol{x} - \boldsymbol{a})}{2\sigma^2} \right) , \quad i \in I \cup I',$$

where $\tilde{C}_i \gg n_i$ is the maximal value of the function, $\boldsymbol{a} = (a_1, a_2)^T$ determines the position of the profile, σ is the standard deviation and

$$(4.2) \qquad f(\boldsymbol{x} - \boldsymbol{a}) = (x_1 - a_1)^2 + \frac{1}{4} \left(\big| |x_2 - a_2| - b \big| + |x_2 - a_2| - b \right)^2 .$$

If $b = 0$, then we have the usual Gaussian profile, for $b > 0$ the maximum extends to a whole line of length b in x_2–direction.

The initial coarse grid used throughout our simulations is shown in Fig. 4.1. Since the region of main solution activity is restricted to the direct neighborhood of the wafer surface – the left hand part of the domain – all graphical presentations given below correspond to the domain $[0, 10^{-4}] \times [0, 10^{-4}]$. All computations were performed on an IBM6000 computer.
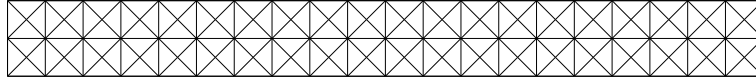
FIG. 4.1. *Coarse grid consisting of 160 triangular elements.*

4.1. Multiple Species Diffusion. Dopant atoms occupy substitutional sites in the silicon crystal lattice, losing (donors such as arsenic and phosphorus) or gaining (acceptors such as boron) at the same time an electron. One fundamental interest in semiconductor devices modelling is to study the interaction of two unequally charged dopants and the influence of the chemical potential. Here, we select arsenic (As) and boron (B). Neglecting heavy doping effects, we get a two–component system with $X_1 = As$ and $X_2 = B$, where both are considered as mobile species, i.e., $I = \{As, B\}$ and $I' = \emptyset$. Thus, the reaction–drift–diffusion model (2.5)–(2.7) reduces to the equations (2.5) and (2.7) with vanishing reaction vector $\boldsymbol{R}$. A detailed description of this classical problem and the various parameters involved can be found in JÜNGLING ET AL. [15].

Particularly, we set $\tilde{C}_{As} = 7 \cdot 10^{20} cm^{-3}$ and $\tilde{C}_B = 2 \cdot 10^{20} cm^{-3}$. Both dopant concentrations have to satisfy homogeneous Neumann boundary conditions.

In Fig. 4.2 the shape of the initial dopant implantations at $950°C$ is visualized. The solutions obtained after thirty minutes show that the boron profile is mainly influenced by the chemical potential while the arsenic concentration is changed only slowly by diffusion, which is in good agreement with the results given in JÜNGLING ET AL. [15]. It can nicely be seen that the dynamic mesh chosen by our adaptive algorithm for $TOL = 0.01$ is well–fitted to the local behaviour of the solution. More grid points are automatically placed in regions of high activity.

4.2. Phosphorus Diffusion. In a second study we use a general pair–diffusion model to simulate phosphorus diffusion under high temperatures $(900°C–1100°C)$. The substitutional phosphorus defects in the silicon crystal lattice are denoted by A. Since a diffusion mechanism based only on the direct interchange with neighbouring silicon atoms turns out to be energetically unfavourable, native point defects called interstitials (I) and vacancies (V) are taken into account. Both can form mobile pairs with phosphorus atoms, designated by AI and AV. Therefore, we set $m = 5$ and use, for a better understanding, instead of $i = 1, \ldots, 5$, the notation $i = I, V, AI, AV, A$, with the mobile species $I = \{I, V, AI, AV\}$ and the immobile species $I' = \{A\}$. The set of permissible reactions $\mathcal{R} = \{(\boldsymbol{\alpha}_i, \boldsymbol{\beta}_i), i = 1, \ldots, 5\}$ we consider can be described by
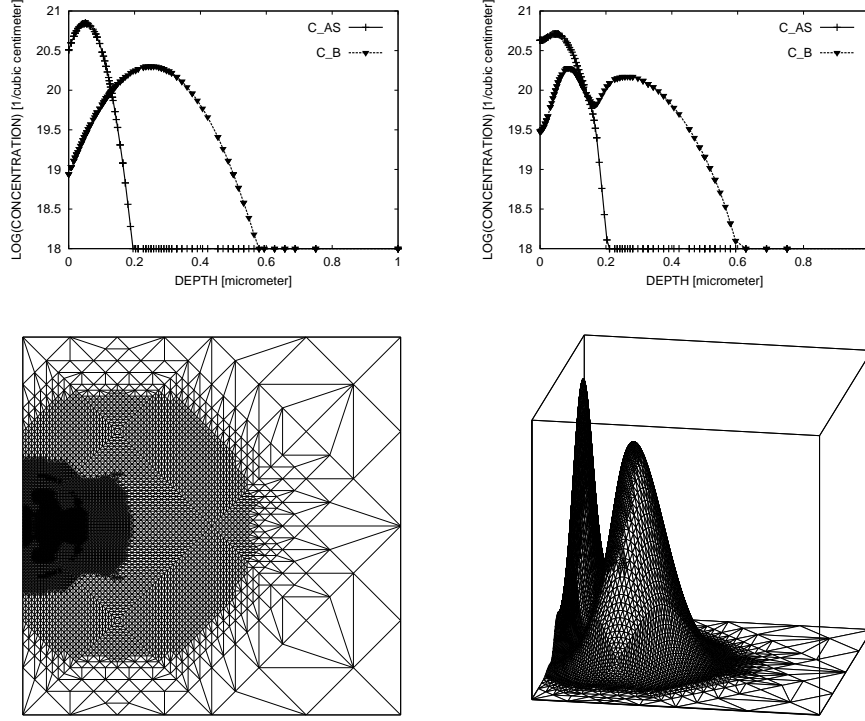
FIG. 4.2. *Arsenic and boron diffusion at* $950°C$. *Top: one–dimensional cuts along* $x_2 = 5 \cdot 10^{-5}$ *through the initial dopant implantations (left) and distributions after* $30\,min$ *(right). Bottom: dynamic mesh (left) and shape of boron at* $t = 30\,min$ *(right).*

$$(4.3) \quad \begin{cases} \boldsymbol{\alpha}_1 = (0,0,0,0,1), & \boldsymbol{\beta}_1 = (1,0,0,1,0)\,; \\ \boldsymbol{\alpha}_2 = (0,0,0,0,1), & \boldsymbol{\beta}_2 = (0,1,1,0,0)\,; \\ \boldsymbol{\alpha}_3 = (0,0,1,0,0), & \boldsymbol{\beta}_3 = (1,0,0,0,1)\,; \\ \boldsymbol{\alpha}_4 = (0,0,0,1,0), & \boldsymbol{\beta}_4 = (0,1,0,0,1)\,; \\ \boldsymbol{\alpha}_5 = (0,0,0,0,0), & \boldsymbol{\beta}_5 = (1,1,0,0,0)\,. \end{cases}$$

The model requires an enormous list of parameters. Most of them are essentially unknown or at least controversial. The complete set of parameters, i.e., the quantities D_i^j, K_i^j, h_i^j, and $K_{\boldsymbol{\alpha}\boldsymbol{\beta}}(\psi)$ can be found in GHADERI & HOBLER [10] and HÖFLER & STRECKER [14].

Particularly, we use Dirichlet boundary conditions at the wafer surface for $i = I, V$, and homogeneous Neumann conditions elsewhere. For the pairs, AI and AV, homogeneous Neumann conditions are taken on the whole boundary. As initial values we use

$$(4.4) \quad C_i(t = 0) = P_i(\psi(t = 0))\,, \quad \text{for all } i \in I.$$

In Fig. 4.3 the evolution of the phosphorus profile and the corresponding dynamic meshes near the wafer surface are plotted. The phosphorus concentration shows its
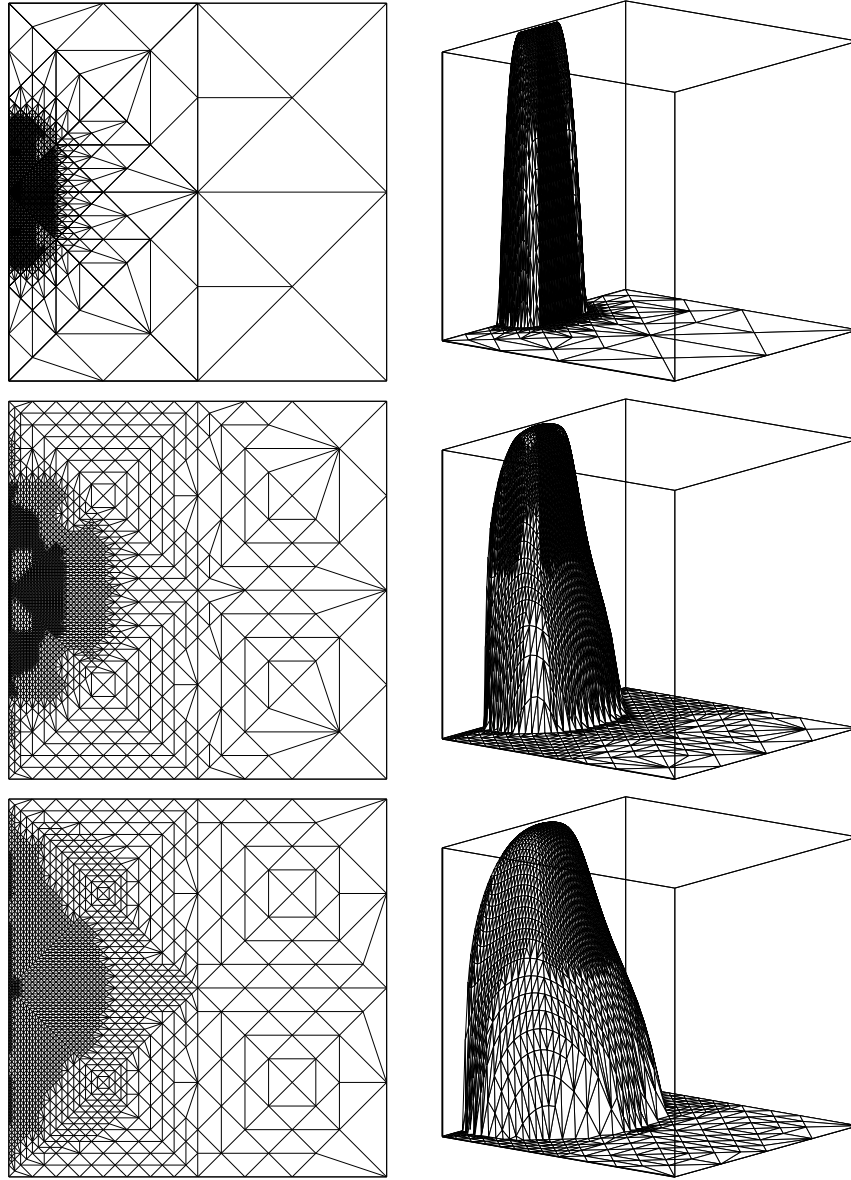
FIG. 4.3. *Phosphorus diffusion at* $900°C$ *with* $\tilde{C}_A = 6 \cdot 10^{20} cm^{-3}$. *Evolution of the dynamic meshes and the phosphorus concentration near the wafer surface at* $t = 0$, $t = 3$, *and* $t = 30\ min$. *The maximal concentration values can be found in Fig. 4.4.*

typical "kink and tail" behaviour, a phenomenon which is known as anomalous diffusion of phosphorus (for a detailed discussion see e.g. RICHARDSON and MULVANEY [22]). Steep gradients are well resolved by the dynamic meshes, not wasting degrees of freedom. Special one–dimensional cuts through the phosphorus concentration at different times and for various peak concentration $\tilde{C}_A$ are shown in Fig. 4.4. We have included the intrinsic case where $\tilde{C}_A = 10^{18} cm^{-3}$. It can be seen clearly that at temperatures much higher than $900°C$ the typical "kink and tail" behaviour vanishes,
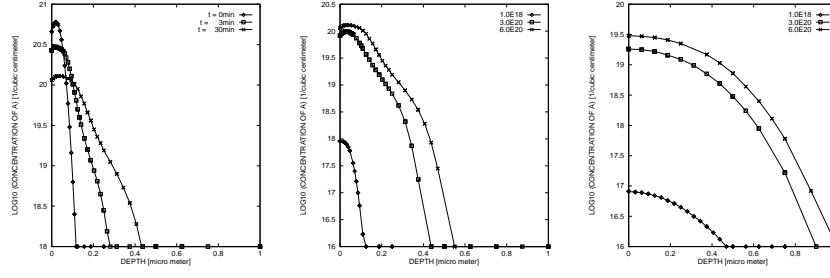
FIG. 4.4. *Phosphorus diffusion. One–dimensional cuts along $x_2 = 5 \cdot 10^{-5}$ through the phosphorus concentration C_A. Left: profiles at different times for $900°C$ and $\tilde{C}_A = 6 \cdot 10^{20} cm^{-3}$. Middle: profiles after 30min for different $\tilde{C}_A$ at $900°C$. Right: profiles after 30min for different $\tilde{C}_A$ at $1100°C$.*
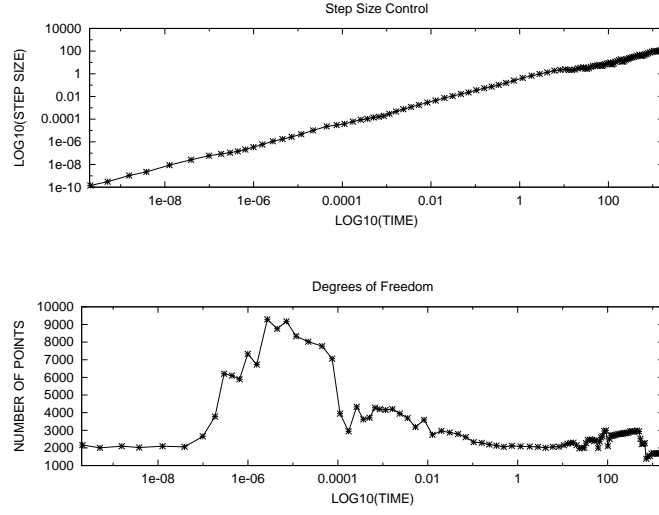

FIG. 4.5. *Phosphorus diffusion at $900°C$ with $\tilde{C}_A = 6 \cdot 10^{20} cm^{-3}$. Evolution of time steps and number of spatial discretization points chosen by ROWDA3 for TOL=0.02.*

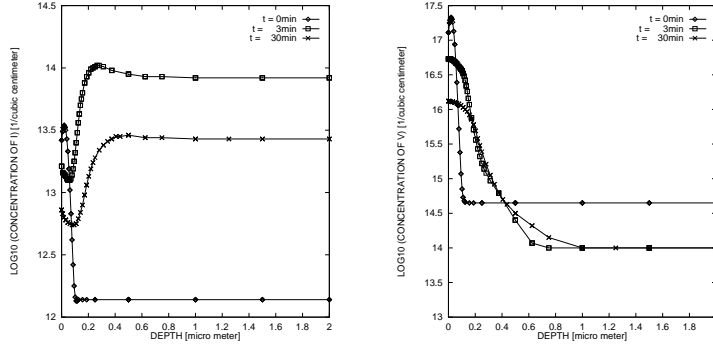FIG. 4.6. *Phosphorus diffusion at $900°C$ with $\tilde{C}_A = 6 \cdot 10^{20} cm^{-3}$. One–dimensional cuts along $x_2 = 5 \cdot 10^{-5}$ through the concentration of interstitials C_I (left) and vacancies C_V (right) at $t = 0$, $t = 3$, and $t = 30\ min$.*

whereas the phosphorus diffusion proceeds faster. All results are in good agreement with those given in the literature [10, 14, 15].

In Fig. 4.5 we have plotted the evolution of time steps and number of grid points used by the adaptive algorithm. The chosen time steps range from $2 \cdot 10^{-10}$ up to $3 \cdot 10^2$ and increase monotonically in time. The spatial dynamics of the system show an irregular behaviour. While approximately 2000 points are sufficient to represent the steep initial contributions, about 9000 nodes around $t = 10^{-5}$ are necessary to guarantee a relative tolerance TOL = 0.02. We have detected that the increase of grid points is caused by the sudden profile change of the interstitials concentration C_I from "concave to convex", which can be seen in Fig. 4.6. Our adaptive algorithm refines the spatial mesh drastically in order to resolve this crucial situation with high accuracy and reliability.

REFERENCES

[1] I. BABUŠKA AND W.C. RHEINBOLDT, *Error estimates for adaptive finite element computations*, SIAM J. Numer. Anal. **15**, 736–754 (1978)

[2] F.A. BORNEMANN, *An adaptive multilevel approach to parabolic equations. I. General theory and 1D implementation*, IMPACT of Comput. in Sci. and Engrg. **2**, 279–317 (1990)

[3] F. A. BORNEMANN, B. ERDMANN, AND R. KORNHUBER, *Adaptive multilevel methods in three space dimensions*, Int. J. Num. Meth. Engrg. **36**, 3187–3203 (1993)

[4] G.F. CAREY, W.B. RICHARDSON, C.S. REED, AND B.J. MULVANEY, *Circuit, Device and Process Simulation, Mathematical and Numerical Aspects*, John Wiley & Sons, New York (1996)

[5] P. DEUFLHARD AND F. BORNEMANN, *Numerische Mathematik II. Integration gewöhnlicher Differentialgleichungen*, de Gruyter Lehrbuch, Berlin, New York (1994)

[6] P. DEUFLHARD, P. LEINEN, AND H. YSERENTANT, *Concepts of an adaptive hierarchical finite element code*, IMPACT of Comput. in Sci. and Engrg. **1**, 3–35, (1989)

[7] B. ERDMANN, J. LANG, AND R. ROITZSCH, *KASKADE Manual, Version 2.0*, TR **93–5**, Konrad–Zuse–Zentrum für Informationstechnik Berlin (1993)

[8] ETH Zurich, *http://www.iis.ee.ethz.ch/software/software.html*

[9] P.M. FAHEY, P.B. GRIFFIN, AND J.D. PLUMMER, *Point defects and dopant diffusion in silicon*, Rev. Mod. Phys. **61**, 290–383 (1989)

[10] K. GHADERI AND G. HOBLER, *Simulation of Phosphorus Diffusion in Silicon using a Pair Diffusion Model with a reduced Number of Parameters*, J. Electrochem. Soc. **142**, 1654–1658 (1995).

[11] A. GLITZKY AND R. HÜNLICH, *Global Estimates and Asymptotics for Electro–Reaction–Diffusion Systems*, Applicable Analysis, **66**, 205–226 (1997)

[12] K. GUSTAFSSON, M. LUNDH, AND G. SÖDERLIND, *A PI stepsize control for the numerical solution of ordinary differential equations*, BIT **28**, 270–287 (1988)

[13] E. HAIRER AND G. WANNER, *Solving ordinary differential equations II, Stiff and Differential-Algebraic Problems*, Springer–Verlag, Berlin, Heidelberg, New York (1991)

[14] A. HÖFLER AND N. STRECKER, *On the Coupled Diffusion of Dopants and Silicon Point Defects*, Technical Report **94/11**, Integrated Systems Laboratory, Swiss Federal Institute of Technology Zurich (1994).

[15] W. JÜNGLING, P. PICHLER, S. SELBERHERR, E. GUERRERO, AND H.W. PÖTZL, *Simulation of Critical IC Fabrication Processes Using Advanced Physical and Numerical Methods*, IEEE Trans. Electron Devices **32**, 156–167 (1985)

[16] J. LANG, *Adaptive FEM for reaction–diffusion equations*, Appl. Numer. Math. **26**, 105–116 (1998)

[17] J. LANG, *Adaptive Multilevel Solution of Nonlinear Parabolic PDE Systems. Theory, Algorithm, and Applications.*, Habilitation thesis, FU Berlin, 1999, ftp://ftp.zib.de/pub/zib-publications/reports/SC–**99–20**.ps

[18] W. MERZ, *Analysis und Numerische Berechnung der Diffusion von Fremdatomen in Homogenen Strukturen*, Habilitationsschrift, TU Munich (1998), SFB 438: TU Munich, Univ. Augsburg, Preprint SFB–**438–9920** (1999)

[19] W. Merz, A. Glitzky, R. Hünlich, and K. Pulverer, *Strong Solutions for Pair Diffusion Models in Homogeneous Semiconductors*, SFB 438: TU Munich, Univ. Augsburg, Preprint SFB-**438**–**9921**, 1–32 (1999)

[20] W. F. Mitchell, *A comparison of adaptive refinement techniques for elliptic problems*, ACM Trans. Math. Software **15**, 326–347 (1989)

[21] P. Pichler, W. Jüngling, S. Selberherr, E. Guerrero, and H.W. Pötzl *Simulation of critical IC–fabrication steps*, IEEE Trans. Electron Devices, **ED**–**32**(10), 1940–1953 (1985)

[22] W.B. Richardson and B.J. Mulvaney, *Nonequilibrium behaviour of charged point defects during phosphorus diffusion in silicon*, J. Appl. Phys., **65**, 2243–2247 (1988)

[23] M. Roche, *Rosenbrock methods for differential algebraic equations*, Numer. Math. **52**, 45–63 (1988)

[24] R. Roitzsch, B. Erdmann, and J. Lang, *The Benefits of Modularization: from KASKADE to KARDOS*, Proceedings of the 14th GAMM-Seminar Kiel on Concepts of Numerical Software, 1998

[25] H. H. Rosenbrock, *Some general implicit processes for the numerical solution of differential equations*, Computer J. (1963), 329–331

[26] K. Strehmel and R. Weiner, *Linear–implizite Runge–Kutta–Methoden und ihre Anwendungen*, Teubner Texte zur Mathematik 127, Teubner Stuttgart, Leipzig (1992)

[27] H. A. van der Vorst, *BI–CGSTAB: A fast and smoothly converging variant of BI–CG for the solution of nonsymmetric linear systems*, SIAM J. Sci. Stat. **13**, 631–644 (1992)